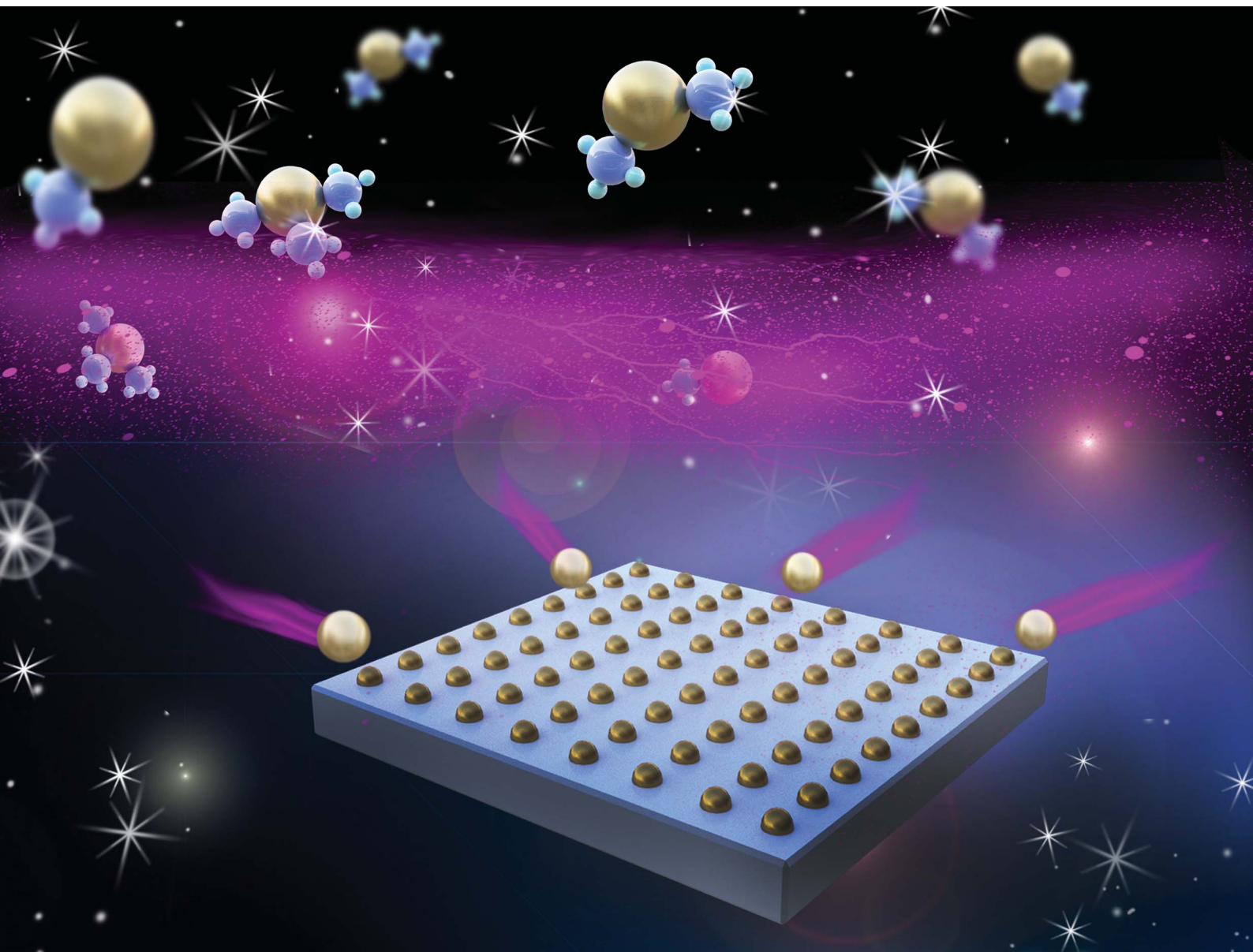


Nanoscale Advances

Volume 2
Number 5
May 2020
Pages 1743-2204

rsc.li/nanoscale-advances



ISSN 2516-0230

PAPER

Xiaojuan Sun, Dabing Li *et al.*
In situ fabrication of Al surface plasmon nanoparticles by metal-organic chemical vapor deposition for enhanced performance of AlGaN deep ultraviolet detectors

Cite this: *Nanoscale Adv.*, 2020, 2, 1854

In situ fabrication of Al surface plasmon nanoparticles by metal–organic chemical vapor deposition for enhanced performance of AlGaN deep ultraviolet detectors

You Wu,^{ab} Xiaojuan Sun,^{ID}*^{ab} Zhiming Shi,^{ab} Yuping Jia,^{ab} Ke Jiang,^{ab} Jianwei Ben,^c Cuihong Kai,^{ab} Yong Wang,^{ab} Wei Lü,^{ID}^{ad} and Dabing Li,^{ID}*^{ab}

Al nanoparticles (NPs) have been proven to be the efficient choice for plasmon enhanced AlGaN-based ultraviolet (UV) photodetectors. Previous studies have mainly been focused on the *ex situ* preparation of Al NPs, but the *in situ* growth of Al NPs is more desired. In this work, we predict the feasibility for *in situ* growth of Al surface plasmon NPs on AlGaN-based UV photodetectors by first-principles calculations, and realized it experimentally by metal–organic chemical vapor deposition. For metal–semiconductor–metal type AlGaN-based photodetectors with *in situ* grown Al surface plasmons, the peak of responsivity was at 288 nm, enhanced 9 times more than that without Al NPs at 10 V bias. The *in situ* growth method of Al NPs in the present work provides an efficient method for improving the performance of AlGaN-based UV photoelectric devices.

Received 10th January 2020
Accepted 22nd February 2020

DOI: 10.1039/d0na00022a

rsc.li/nanoscale-advances

Introduction

AlN and AlGaN-based materials are typical representatives of third-generation semiconductor materials with direct transition energy bands and wide band gap, as well as excellent thermal and chemical stability, which are extensively applied to high-performance ultraviolet (UV) and deep-ultraviolet (DUV) photoelectric devices, such as photodetectors (PDs), light emitting diodes (LEDs) and laser diodes (LDs).^{1–6} Among them, AlGaN-based UV emitters and detectors show potential application in biomedical, sterilization, flame detection and missile warning,^{7,8} and they have received extensive attention. Different types of AlGaN-based UV photodetectors with promising performance have been demonstrated, such as Schottky type, metal–semiconductor–metal (MSM) type, p–n/p–i–n type and avalanche detectors. However, due to the constraints of material quality and doping difficulties, the device performance is currently far below expectations. Recently, surface plasmon (SP) enhancement by metal nanoparticles (NPs) has provided a new

approach to obtain high performance UV optoelectronic devices.

Surface plasmon resonance would occur when the frequency of the incident light wave coincides with the oscillation frequency of the electrons. The energy of the electromagnetic field is then effectively converted into the collective vibration energy of the free electrons of metal nanostructures, resulting in an enhanced electromagnetic field. Surface plasmon enhancement has extensive applications in optoelectronic devices,^{9,10} biological sensors,^{11,12} and photocatalytic and¹³ and high resolution imaging.^{14,15}

In theory, the metal nanoparticles surface plasmon effect is related to its quality factor, $Q_m = -\text{Re}\epsilon_m(\omega)/\text{Im}\epsilon_m(\omega)$, where $\text{Re}\epsilon_m(\omega)$ and $\text{Im}\epsilon_m(\omega)$ is the real and imaginary part of the permittivity.^{16,17} A larger Q_m indicates a stronger plasmon effect in this wavelength. According to their quality factors, Au^{18,19} and Ag^{20,21} can be used for visible and near-UV optoelectronic device enhancement, but Al is a good choice to enhance the performance of UV and DUV optoelectronic devices.^{22–24} In addition, Al SPs have the advantages of low price and a wide range of natural sources. However, the fabrication of Al SPs is difficult due to the high viscosity of the Al material. For Au and Ag NPs, they are easily achieved by rapid thermal annealing after vacuum evaporation. But Al films are usually formed at the beginning instead of Al NPs, when using vacuum evaporation. Even though the Al films are treated by a rapid thermal annealing method, Al NPs cannot be obtained.

Currently major methods for preparing Al NPs as SPs are an *ex situ* preparation strategy including optimized vacuum

^aState Key Laboratory of Luminescence and Applications, Changchun Institute of Optics, Fine Mechanics and Physics, Chinese Academy of Sciences, Changchun 130033, People's Republic of China. E-mail: sunxj@ciomp.ac.cn; lidb@ciomp.ac.cn

^bCenter of Materials Science and Optoelectronics Engineering, University of Chinese Academy of Sciences, Beijing 100049, People's Republic of China

^cCollege of Materials Science and Engineering, Shenzhen University, Shenzhen 518071, People's Republic of China

^dKey Laboratory of Advanced Structural Materials, Ministry of Education, Changchun University of Technology, Changchun 130012, People's Republic of China



evaporation,²³ electron beam lithography (EBL),²⁵ nanosphere lithography (NSL),^{24,26} and nanoimprinting,²⁷ which would cause pollution at the interface between Al NPs and AlGaN, affecting the transfer of energy and carriers from metal plasmons to semiconductor epi-layers. Moreover, Al NPs by *ex situ* preparation can only be fabricated on the surface of the oriented samples. Since the SP enhancement effect decays exponentially in the direction perpendicular to the interface, it is difficult for *ex situ* fabricated Al SPs to penetrate the active region and thus limits the applications of the plasmon enhancement effect. To narrow the distance between the NPs and the active layer, M. Razeghi *et al.*²⁸ used a selective etching process to form holes near the multiple quantum wells (MQWs) and deposited Al in the resulting holes to obtain plasmon enhanced UV-LEDs. However, this method is complicated, time consuming and costly, and will induce additional defects. Therefore, an effective *in situ* growth method of Al SPs on AlGaN-based materials is highly desired.

In this study, we report a method of *in situ* growth of Al nanostructures on AlGaN epi-layers by metal–organic chemical vapor deposition (MOCVD), and confirm its excellent plasmon enhancement effect for AlGaN-based MSM type UV PDs. We proposed the novel idea of the *in situ* growth of Al NPs on AlGaN epi-layers by MOCVD according to the growth kinetics process. Both theoretical calculations and experiments have been studied to confirm the feasibility. Furthermore, the significant enhancement in responsivity for AlGaN-based UV photodetectors with *in situ* grown Al NPs was verified.

Experimental section

1. Growth details of materials

The 1 μm thick unintentional doping $\text{Al}_{0.4}\text{Ga}_{0.6}\text{N}$ epi-layer was grown on a (0001) sapphire substrate by high-temperature MOCVD at 1180 $^{\circ}\text{C}$. Before the AlGaN layer was deposited, the substrate was first heated to 1230 $^{\circ}\text{C}$ under a H_2 atmosphere to remove surface contamination and then a 1 μm AlN template layer was grown by a two-step growth method. Trimethylgallium (TMGa), trimethylaluminum (TMAI) and ammonia (NH_3) were used as Ga, Al and N precursors, respectively. After AlGaN layer growth, all precursors were stopped and only the carrier gas (H_2) was used to evacuate the gas chamber. Then, the temperature was decreased to 950 $^{\circ}\text{C}$, and the Al precursor was separately introduced to fabricate Al NPs. This process is termed as “*in situ* NP growth” and the schematic diagram of the growth process is illuminated in Fig. 1(a and b). Four samples were grown by varying the growth time of Al (0 s, 15 s, 30 s, and 60 s) and named Sample A, B, C, and D, respectively.

2. Device fabrication

The Ni/Au (50 nm/20 nm) Schottky contacts were fabricated by vacuum evaporation for the interdigitated contacts of the AlGaN MSM type detector and then the samples were treated by rapid thermal annealing at 450 $^{\circ}\text{C}$ for 180 s. The fingers of the interdigitated contacts were 100 μm in length and 10 μm in width with a spacing of 10 μm . These devices were fabricated by

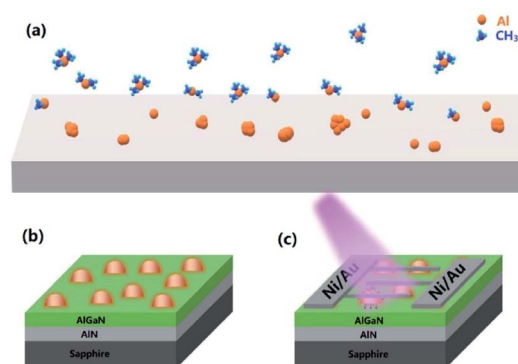


Fig. 1 The schematic diagram of the growth process (a), result (b) and device structure (c).

standard photolithography and lift-off process. The device structure diagram is shown in Fig. 1(c).

3. Characterization

The surface topography of the AlGaN layer with *in situ* Al NPs was characterized by using the tapping mode of an atomic force microscope (AFM) (Bruker multimode 8). X-ray photoelectron spectroscopy (XPS) measurements were carried out on a spectrometer (VG ESCALAB MKII) with Al $K\alpha$ X-ray radiation as the excitation source. To study the optical spectral response of the devices, a UV-enhanced Xe arc lamp was used as the light source and a UV-enhanced Si detector was used for calibrating. The incident light was modulated by using a mechanical chopper while the lock-in amplifier was used to record the photocurrent. The current–voltage (I – V) performance of the AlGaN-based detectors was measured by using a Keithley 6487 electrometer.

4. First-principles calculations

First-principles calculations were performed by employing the generalized gradient approximation (Perdew–Burke–Ernzerhof parametrization, PBE) and a projector-augmented wave method as implemented in the Vienna *Ab initio* Simulation Package.²⁹ The vdW interaction^{30,31} was included in the calculations. A plane-wave basis setting with a kinetic energy of 500 eV was used. We used gamma-only k -points in the calculations. The force and total energy convergence thresholds were set to 0.015 eV \AA^{-1} and 10^{-5} eV, respectively. Here, a four-layer rectangle $\text{Al}_{0.5}\text{Ga}_{0.5}\text{N}$ supercell containing 240 atoms was used in our calculations. The in-plane lattice parameters of the supercell were larger than 16 \AA and the vacuum slabs were thicker than 15 \AA to avoid artificial interaction of the periodic images. The N-surface was passivated by hydrogen, and the dangling metal-surface was fully optimized.

Results and discussion

According to previous reports on the kinetics of AlGaN-based material growth by MOCVD,³² the metal organic source is decomposed by the heated substrate in a reaction chamber. The decomposition reaction of TMAI could be expressed as follows:



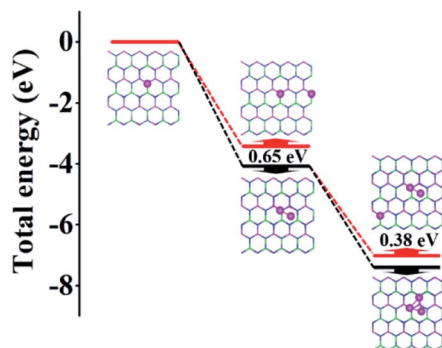
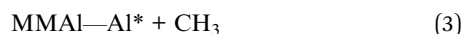
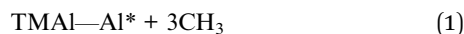


Fig. 2 The total energy of Al atoms adsorbed one by one on the $\text{Al}_{0.5}\text{Ga}_{0.5}\text{N}$ surface.



wherein MMAI represents AlCH_3 and TMAI represents $\text{Al}(\text{CH}_3)_3$. In the traditional strategy, the introduction of TMAI has to be accompanied by NH_3 to grow the AlGaN epi-layer. In the present work, we try to introduce the Al precursor alone without NH_3 supply after AlGaN layer growth for the *in situ* fabrication of Al SPs. However, as mentioned above, the high viscosity of Al is a challenge for the fabrication of Al SPs.

To demonstrate the clustering behavior of Al atoms on the AlGaN surface, we calculated the total energy of Al atoms adsorbed one by one on the $\text{Al}_{0.5}\text{Ga}_{0.5}\text{N}$ surface. The Al atom adsorption was an exothermic process indicating the stability of the structures. In Fig. 2, we find that the single Al atom preferred binding on the top of N atoms due to the Coulomb interaction. Next, we put one more Al atom close or far from the first one to form an Al dimer or isolated Al atoms respectively. The dimer adsorbed structure exhibited lower energy by 0.65 eV than that of the isolated adsorbed structure. When we further added the third Al atom, the additional Al atom adsorbed

structure also preferred clustering rather than separate distribution by 0.38 eV. Therefore, the Al cluster was easily formed and can be stably adsorbed on the $\text{Al}_{0.5}\text{Ga}_{0.5}\text{N}$ surface.

The experiment obtained a similar phenomenon consistent with the calculation results. In this study, four “*in situ* NP growth” samples were prepared by varying the growth times of 0 s, 15 s, 30 s, and 60 s, named Sample A, B, C, and D, respectively, *i.e.*, Sample A is an AlGaN epi-layer without *in situ* NPs. Fig. 3 shows the surface morphology of these four samples in an area of $1 \mu\text{m} \times 1 \mu\text{m}$ by using a tapping-mode AFM. A typical stepped surface topography of the AlGaN epi-layer (Sample A) is shown in Fig. 3(a), while nano-islands are shown on the AlGaN layers with *in situ* grown NP (Sample B, C, and D) as shown in Fig. 3(b–d). Fig. 3(e–h) show the 3D morphologies of Sample A, B, C, and D respectively. The average diameters of NPs on Sample B, C, and D are 20 nm, 40 nm, and 60 nm, respectively. The results show that the diameters of the nano-islands and the thickness of the NP layer increase with the increasing growth time. During the *in situ* growth process, the Al precursor decomposed and nucleated on the heated substrate. The subsequent Al precursors decomposed and expanded based on these nucleation sites, which is consistent with the evolution of growth kinetics in MOCVD growth by previous studies.³³ When the size is enlarged and merged, a quasi-continuous layer would also be formed.

To determine the composition of the surface nano-islands, an XPS test was performed. Fig. 4(a) shows the XPS survey scan spectrum of the sample without NPs, that is, the AlGaN epi-layer, while Fig. 4(b) shows that of the sample with NPs with 30 s *in situ* growth. Compared with those of the AlGaN epi-layer without NPs, the peaks of N 1s, Ga 3d and Ga 2p core-levels are significantly reduced while O 1s is increased in Fig. 4(b). However, the intensity of the Al 2p core-level peak does not change obviously, which means that there is almost no Ga and N in these NPs, but Al is present. The XPS narrow region scan results of the Al 2p and O 1s core-levels are shown in Fig. 4(c and d). The chemical shift of the Al 2p peak position is distinct, and the binding energy (BE) shifts from 73.3 eV to 74.1 eV correspond to the Al–N bond³⁴ and Al–O bond³⁵ respectively. Moreover, a shoulder located at the left side of the

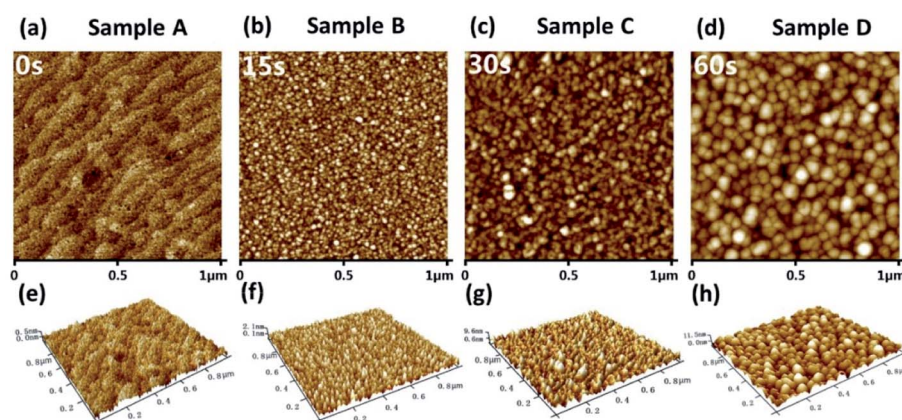


Fig. 3 AFM images of the four samples with different *in situ* NP growth times. (a–d) are the planar views, and (e–h) are the 3D views of the four samples, respectively.



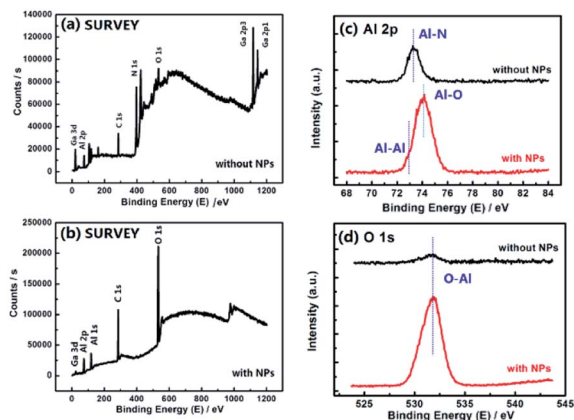


Fig. 4 (a and b) are XPS survey scan spectra of the samples with and without surface NPs. (c) is Al 2p core-level XPS spectra, and (d) is O 1s core-level XPS spectra of the samples with and without NPs.

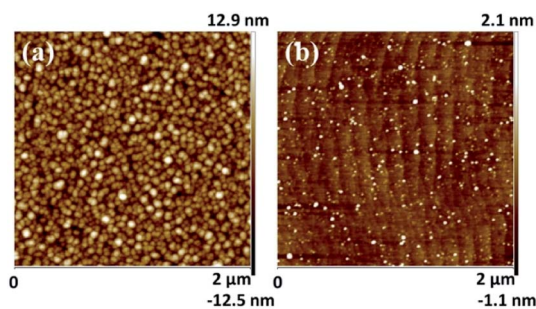


Fig. 5 The AFM surface morphology of *in situ* NP growth samples before (a) and after (b) H_3PO_4 etching.

major peak could be observed and might be due to metallic Al (Al–Al bond, at ~ 72.9 eV (ref. 36)), indicating that Al-clusters were formed on the AlGaIn epi-layers. Fig. 4(d) also indicates the existence of an O–Al bond (~ 531.6 eV).³⁷ The XPS spectra demonstrate that the composition of nano-islands could be Al with an oxide film, Al_2O_3 (usually ~ 3 nm).

To further verify the existence of Al NPs, the samples with NPs were etched with H_3PO_4 solution at 65°C for 10 minutes. Fig. 5(a and b) show the tapping-AFM surface topography of a typical sample with *in situ* grown NPs for 60 s before and after H_3PO_4 etching, respectively. The etched sample in Fig. 5(b) shows a significant step shape surface topography, like Sample A in Fig. 3(a), which proves the reaction between the nano-islands and the H_3PO_4 solution. Considering the growth process in MOCVD, the NPs can be confirmed to be Al nanoparticles again.

Here we use MSM-type AlGaIn-based UV PDs to verify the enhancement of *in situ* grown Al NPs. The schematic of the device structure is shown in the inset of Fig. 6(b). Four PDs (PD A, PD B, PD C and PD D) were fabricated, corresponding to the different *in situ* Al NP growth times (0 s, 15 s, 30 s, and 60 s). Fig. 6 illustrates the dark current (I_{dark}) and the spectral responsivity under 10 V bias of these detectors. For PD B, with 15 s *in situ* NP growth, the I_{dark} is slightly lower than that without NPs, which could be attributed to the passivation effect of Al_2O_3 ,³⁸ while for PD C (30 s)

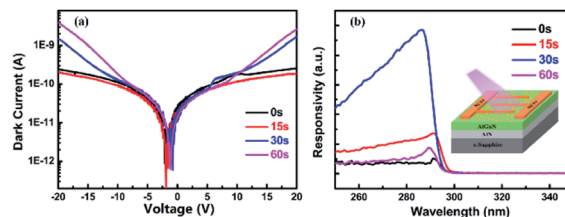


Fig. 6 (a) Dark current–voltage (I – V) curves of AlGaIn MSM detectors with and without Al NPs. (b) Responsivity of MSM photodetectors with and without Al NPs under 10 V bias. A schematic of the device structure is shown in the inset of (b).

and PD D (60 s), the I_{dark} is slightly increased due to the lower Schottky contact height between the Ni/Au electrons and the AlGaIn epilayer because of the Al NP increase.

The spectral response of the AlGaIn PDs with and without *in situ* grown Al NPs was also studied. For samples with 0 s and 15 s growth time, the responsivity peaks at approximately 290 nm. And for samples with 30 s and 60 s growth time, the peaks are slightly blue shifted, at 288 nm, which could be related to the plasmon effect of Al on the surface, consistent with the results reported previously.^{23,39} For the 15 s sample, no significant blue shift occurs in the cut-off wavelength due to the small diameter of the NPs (less than 20 nm).²³ As shown in Fig. 6(b), all PDs with *in situ* grown Al NPs have higher responsivity compared with PDs without NPs. The peak responsivity of PD C (30 s) is enhanced over 9 times that of PD A. Compared with our previous work, in which the responsivity of the AlGaIn PD with *ex situ* Al NPs was enhanced nearly 2 times more than that without Al NPs,²³ the *in situ* preparation of Al NPs is superior. Further deposition of Al induces deterioration in photoresponsivity (PD D). As shown in Fig. 3, the average size of Al NPs increases with the increasing deposition time, indicating the size of Al NPs affects the performance improvement, and the optimized deposition time in the present work is 30 s.

The enhancement of photoresponsivity might have resulted from these possible mechanisms: (i) the *in situ* Al NP surface plasmon resonance induces local electric field enhancement,²¹ and thus generates more carriers as well as accelerates the separation of the carriers, leading to the enhancement of the responsivity. (ii) Al NPs generate hot carriers, which are emitted across the Schottky barrier and injected into the conduction band of the AlGaIn layer, leading to the photocurrent increase. The hot carrier effect is especially noticeable when the size of the NPs is small.^{40,41} Therefore, in PD B, the main enhancement mechanism is the hot carrier phenomenon. (iii) The *in situ* grown NPs and the AlGaIn interface have less pollution, which could improve the transfer of energy and carriers from metal NPs to the semiconductor. This might be the main reason for the better improvement of photoresponsivity in this work than in the *ex situ* prepared Al NPs.

Conclusion

In conclusion, we have verified the feasibility of the *in situ* growth of Al NPs by MOCVD from both theoretical calculations



and experiments, and achieved photoresponsivity enhanced AlGaIn-based UV PDs by *in situ* grown Al NP surface plasmons. The peak photoresponsivity of PDs was enhanced by 9 times more than that of the device without Al NPs at 288 nm under 10 V bias, which is better than the enhancement of AlGaIn-based UV PDs by *ex situ* prepared Al NPs previously. *In situ* growth of Al NPs not only causes surface plasmon resonance, but also reduces energy and carrier loss at the interface because of less contamination. Our work broadens the application of Al surface plasmon enhanced AlGaIn-based UV and DUV photoelectric devices.

Conflict of interest

The authors declare no competing financial interest.

Acknowledgements

This work was supported by the National Key R&D Program of China [2016YFB0400101], the National Science Fund for Distinguished Young Scholars [61725403], the National Natural Science Foundation of China [61574142, 61874118, 61827813, and 61704171], the Key Program of the International Partnership Program of CAS [181722KYSB20160015], the Jilin Provincial Science & Technology Department [20180201026GX], and the Youth Innovation Promotion Association of CAS.

References

- 1 M. Sajjad, W. M. Jadwisieniczak and P. Feng, *Nanoscale*, 2014, **6**, 4577–4582.
- 2 H. Durmaz, D. Nothorn, G. Brummer, T. D. Moustakas and R. Paiella, *Appl. Phys. Lett.*, 2016, **108**, 201102.
- 3 D. Y. Kim, J. H. Park, J. W. Lee, S. Hwang, S. J. Oh, J. Kim, C. Sone, E. F. Schubert and J. K. Kim, *Light: Sci. Appl.*, 2015, **4**, e263.
- 4 T. A. Growden, W. Zhang, E. R. Brown, D. F. Storm, D. J. Meyer and P. R. Berger, *Light: Sci. Appl.*, 2018, **7**, 17150.
- 5 Z. Bryan, I. Bryan, S. Mita, J. Tweedie, Z. Sitar and R. Collazo, *Appl. Phys. Lett.*, 2015, **106**, 232101.
- 6 H. Yoshida, Y. T. Akagi, M. Kuwabara, H. Amano and H. Kan, *Jpn. J. Appl. Phys.*, 2007, **46**, 5782–5784.
- 7 D. Li, K. Jiang, X. Sun and C. Guo, *Adv. Opt. Photonics*, 2018, **10**, 43–110.
- 8 E. Muñoz, *Phys. Status Solidi B*, 2007, **244**, 2859–2877.
- 9 C.-Y. Cho, Y. Zhang, E. Cicek, B. Rahnema, Y. Bai, R. McClintock and M. Razeghi, *Appl. Phys. Lett.*, 2013, **102**, 211110.
- 10 S. Butun, N. A. Cinel and E. Ozbay, *Nanotechnology*, 2012, **23**, 444010.
- 11 V. A. Briand, V. Thilakarathne, R. M. Kasi and C. V. Kumar, *Talanta*, 2012, **99**, 113–118.
- 12 J. Homola, *Chem. Rev.*, 2008, **108**, 462–493.
- 13 C. Clavero, *Nat. Photonics*, 2014, **8**, 95.
- 14 J. S. Clausen, E. Højlund-Nielsen, A. B. Christiansen, S. Yazdi, M. Grajower, H. Taha, U. Levy, A. Kristensen and N. A. Mortensen, *Nano Lett.*, 2014, **14**, 4499–4504.
- 15 S. J. Tan, L. Zhang, D. Zhu, X. M. Goh, Y. M. Wang, K. Kumar, C.-W. Qiu and J. K. W. Yang, *Nano Lett.*, 2014, **14**, 4023–4029.
- 16 Y. Wu, X. Sun, Y. Jia and D. Li, *Chin. Phys. B*, 2018, **27**, 26101.
- 17 X. Jiao and S. Blair, *Opt. Express*, 2012, **20**, 29909–29922.
- 18 Y.-H. Su, Y.-F. Ke, S.-L. Cai and Q.-Y. Yao, *Light: Sci. Appl.*, 2012, **1**, e14.
- 19 M.-K. Kwon, J.-Y. Kim and S.-J. Park, *J. Cryst. Growth*, 2013, **370**, 124–127.
- 20 D. Li, X. Sun, H. Song, Z. Li, Y. Chen, H. Jiang and G. Miao, *Adv. Mater.*, 2012, **24**, 845–849.
- 21 D. Li, X. Sun, Y. Jia, M. I. Stockman, H. P. Paudel, H. Song, H. Jiang and Z. Li, *Light: Sci. Appl.*, 2017, **6**, e17038.
- 22 N. Gao, K. Huang, J. Li, S. Li, X. Yang and J. Kang, *Sci. Rep.*, 2012, **2**, 816.
- 23 G. Bao, D. Li, X. Sun, M. Jiang, Z. Li, H. Song, H. Jiang, Y. Chen, G. Miao and Z. Zhang, *Opt. Express*, 2014, **22**, 24286.
- 24 W. Zhang, J. Xu, W. Ye, Y. Li, Z. Qi, J. Dai, Z. Wu, C. Chen, J. Yin, J. Li, H. Jiang and Y. Fang, *Appl. Phys. Lett.*, 2015, **106**, 021112.
- 25 O. Lecarme, Q. Sun, K. Ueno and H. Misawa, *ACS Photonics*, 2014, **1**, 538–546.
- 26 G. H. Chan, J. Zhao, G. C. Schatz and R. P. V. Duyne, *J. Phys. Chem. C*, 2008, **112**, 13958–13963.
- 27 A. Boltasseva, *J. Opt. A: Pure Appl. Opt.*, 2009, **11**, 114001.
- 28 C.-Y. Cho, Y. Zhang, E. Cicek, B. Rahnema, Y. Bai, R. McClintock and M. Razeghi, *Appl. Phys. Lett.*, 2013, **102**, 211110.
- 29 D. L. Winn, M. J. Hale, T. J. Grassman, J. Z. Sexton and A. C. Kummel, *J. Chem. Phys.*, 2007, **127**, 134705.
- 30 V. Barone, M. Casarin, D. Forrer, M. Pavone, M. Sambri and A. Vittadini, *J. Comput. Chem.*, 2009, **30**, 934–939.
- 31 S. Grimme, *J. Comput. Chem.*, 2006, **27**, 1787–1799.
- 32 T. G. Mihopoulos, V. Gupta and K. F. Jensen, *J. Cryst. Growth*, 1998, **195**, 733–739.
- 33 J. Ma, Q. Zhuang, G. Chen, C. Huang, S. Li, H. Wang and J. Kang, *J. Phys. Chem. A*, 2010, **114**, 9028–9033.
- 34 T. Hagio, A. Takase and S. Umeyashiki, *J. Mater. Sci. Lett.*, 1992, **11**, 878–880.
- 35 H. He, K. Alberti, T. L. Barr and J. Klinowski, *J. Phys. Chem.*, 1993, **97**, 13703–13707.
- 36 C. Hinnen, D. Imbert, J. M. Siffre and P. Marcus, *Appl. Surf. Sci.*, 1994, **78**, 219–231.
- 37 B. R. Strohmeier, *Surf. Sci. Spectra*, 1994, **3**, 135–140.
- 38 X. Sun, D. Li, H. Jiang, Z. Li, H. Song, Y. Chen and G. Miao, *Appl. Phys. Lett.*, 2011, **98**, 121117.
- 39 J. Yin, Y. Li, S. Chen, J. Li, J. Kang, W. Li, P. Jin, Y. Chen, Z. Wu, J. Dai, Y. Fang and C. Chen, *Adv. Opt. Mater.*, 2014, **2**, 451–458.
- 40 P. Christopher and M. Moskovits, *Annu. Rev. Phys. Chem.*, 2017, **68**, 17.
- 41 F. Wang and N. A. Melosh, *Nano Lett.*, 2011, **11**, 5426–5430.

